

Jets and QCD

JET PRODUCTION AND QCD IN THE UA1 EXPERIMENT

UA1 Collaboration, CERN, Geneva, Switzerland

Aachen - Amsterdam (NIKHEF) - Annecy (LAPP) - Birmingham - CERN -
Harvard - Helsinki - Kiel - London (Queen Mary College) - Paris
(Coll. de France) - Riverside - Rome - Rutherford Appleton Lab. -
Saclay (CEN) - Vienna - Wisconsin Collaboration

(Presented by W. Scott)

1. INTRODUCTION

This paper presents results of the comparison of three-jet and two-jet cross-sections in $p\bar{p}$ collisions measured in the UA1 apparatus at the CERN Super Proton Synchrotron (SPS) $p\bar{p}$ Collider. The motivation for this study stems from the need for a better understanding of general multijet production (≥ 3 jets) in high-energy $p\bar{p}$ collisions. In quantum chromodynamics (QCD), multijet events can occur as a result of strong radiative corrections to elastic parton-parton scattering processes. At sufficiently high subprocess c.m.s. energies, single QCD bremsstrahlung should become the dominant mechanism for the production of three-jet events. In this paper the bremsstrahlung hypothesis is tested by comparing the measured three-jet differential cross-section, at the highest available energies, with the predictions of the single bremsstrahlung formulae. The observed relative rate of three-jet and two-jet events is used to obtain information on the value of the strong interaction coupling constant α_s .

Results on the two-jet cross-section measured in high-energy $p\bar{p}$ collisions have been given previously^{1,2}. It has been found that the measured subprocess cross-sections follow closely the

leading-order QCD predictions for (massless) final-state partons³⁾ which, neglecting constant and slowly varying factors, may be written:

$$d\sigma/d \cos \theta \approx (\alpha_s^2/\hat{s}) (1 - \cos \theta)^{-2}, \quad (1)$$

where \hat{s} is the subprocess c.m.s. energy squared and $\cos \theta$ is the c.m.s. scattering angle. In particular, the characteristic (Rutherford) angular dependence $[(1 - \cos \theta)^{-2}]$ has been checked directly by plotting the c.m.s. angular distribution of the jet pairs.

For three final-state (massless) partons the final-state parton configuration, at fixed subprocess c.m.s. energy, is specified by four independent variables. The leading-order QCD predictions for the subprocess cross-sections are given by:

$$d^4\sigma/dx_3 dx_4 d \cos \theta_3 d\psi = (1/32\pi^2)|M|^2, \quad (2)$$

where, neglecting constant and slowly varying factors, the spin- and colour-averaged matrix element squared $|M|^2$ may be written:

$$|M|^2 \approx (\alpha_s^3/\hat{s}) [x_{T_3}^2 x_{T_4}^2 x_{T_5}^2 (1 - x_3)(1 - x_4)(1 - x_5)]^{-1} \quad (3)$$

In Eqs. (2) and (3) the x_i ($i = 3, 4, 5$) are the energies (or momenta) of the outgoing partons, ordered so that $x_3 > x_4 > x_5$ and scaled to the total subprocess c.m.s. energy such that $x_3 + x_4 + x_5 = 2$; θ_i is the angle between the parton i and the beam direction ($x_{T_i} = x_i \sin \theta_i$), and ψ is the angle between the plane defined by partons 4 and 5 and the plane defined by the beam direction and parton 3 (see Fig. 1). The exact (leading-order) expressions for $|M|^2$ for the various incoming and outgoing parton combinations (e.g. $gg \rightarrow ggg$, $qg \rightarrow qgg$, etc.) have been given in a simple form by Berends et al.⁴⁾. An important feature of the three-parton cross-sections is that for three-parton configurations which approach two-parton configurations, i.e. $x_3, x_4 \rightarrow 1$ or $x_{T_i} \rightarrow 0$, the cross-sections become large as a result of final- (or initial-) state bremsstrahlung processes. Naturally the comparison of theory with experiment must be restricted to a region of phase space where all the jets are well separated from each other and from the beams, and in which the theoretical cross-sections are finite and relatively slowly varying.

2. TWO-JET CROSS-SECTION

The present analysis is based on data from the 1983 Collider run. The initial data sample comprised all jet triggers corresponding to an integrated luminosity of $\approx 100 \text{ nb}^{-1}$. The 1983 jet trigger required ≥ 1 localized transverse energy deposition anywhere in the central calorimetry (pseudorapidity $|\eta| < 3$). The trigger E_T threshold was set at 15, 20, or 25 GeV, depending on the running conditions. For this analysis the data were passed through a filter program which duplicated the trigger algorithm selecting all events with localized transverse energy $E_T > 30$ GeV. Events involving two interactions in the same SPS bunch crossing and events with associated beam-halo hits are removed from the sample by imposing requirements on the total energy ($E_{\text{tot}} < 600$ GeV) and on the magnitude of the missing E_T vector ($\vec{E}_T^{\text{miss}} < 2.5$ st. dev.). The jet 4-momenta are computed by combining the calorimeter hits, using the UA1 jet algorithm, and correcting for various apparatus effects and losses as discussed previously¹⁾. As a function of the corrected transverse momentum (p_T) of the highest transverse momentum jet, the efficiency of the filter selection, per event, is $\geq 90\%$ for $p_T > 45$ GeV.

All events with ≥ 2 jets defined by the jet algorithm are considered as two-jet candidates. Additional jets apart from the two highest p_T jets are simply ignored. For two-jet events the subprocess c.m.s. energy is taken to be the two-jet mass ($\sqrt{\hat{s}} = m_{2J}$) computed using the full (corrected) 4-vectors (i.e. including the jet masses) of the two highest- p_T jets. The c.m.s. scattering angle θ is defined relative to the incoming parton axis, taken to be the average beam direction in the two-jet rest frame. To ensure good trigger/filter efficiency for the two-jet sample, we require $\cos \theta < 0.8$ and $m_{2J} > 150$ GeV.

The final two-jet sample comprises 1142 events, satisfying the two-jet cuts. The angular distribution for these events, plotted as a function of $\cos \theta$, is consistent with previous data^{1,2)} and is shown in Fig. 2a. In Fig. 2b the same angular distribution has been plotted as a function of the variable χ [$\chi = (1 + \cos \theta)/(1 - \cos \theta)$]⁶⁾. This variable has the property that if Eq. (1) holds exactly, then the χ -distribution will be essentially flat for $\chi \geq 2$. In Fig. 2 the theoretical curves, which have been normalized to the data, have been calculated using the exact (leading-order) QCD formulae³⁾, averaging appropriately over the contributing subprocesses. The relative importance of the various incoming parton combinations has been inferred on the basis of quark (and gluon) structure functions measured in deep-inelastic scattering experiments⁷⁾. Averaged over the mass range 150 to 250 GeV, the proportion of two-jet events corresponding to the incoming parton combinations $gg:qg:q\bar{q}$ is estimated to be $\approx 12\%: 52\%: 36\%$, respectively. Since the dominant subprocesses have very similar angular distributions, in practice this averaging has a rather small effect.

In Fig. 2 the broken curves represent the theoretical prediction assuming exact scaling, and the solid curves indicate the effect of various scale-breaking corrections. The scale-breaking corrections include the Q^2 -dependence of α_s , through the factor α_s^2 in Eq. (1) and the Q^2 -dependence of the effective structure function calculated assuming $Q^2 = -\hat{t}$ and taking the QCD scale parameter $\Lambda = 0.2$ GeV. As a consequence of the large values of Q^2 ($Q^2 \geq 4000$ GeV²) the value of Λ is poorly constrained by the present data. Assuming $Q^2 = -\hat{t}$ we obtain $-3.7 < \ln(\Lambda/m) < +0.1$ with 90% confidence (where m is the mass of the proton). We conclude that scale-breaking corrections are required to fit the data, and furthermore that the effective Q^2 -scale, which is not known theoretically *a priori*⁸⁾, is dependent on the scattering angle and consistent with $Q^2 = -\hat{t}$. A similar observation has previously been made in an ISR experiment⁹⁾.

3. THREE-JET CROSS-SECTION

The three-jet sample is selected from all events with ≥ 3 jets defined by the jet algorithm. For each event the full (corrected) jet 4-vectors are transformed into the rest frame of the three highest- p_T jets. Additional jets, apart from the three highest p_T jets, are ignored. The energies of the jets in the three-jet rest frame are used to compute the x_i and to define the jet ordering (jet-3, jet-4, etc.). The angles θ_3 and ψ are computed using the jet directions and the direction of the incoming parton axis, taken to be the average beam direction, in the three-jet rest frame.

To ensure that all three jets are well separated from each other and from the beams, the following cuts are applied to define the three-jet sample:

i) $x_3 < 0.9$. This cut guarantees that jet-4 and jet-5 are well separated in angle in the subprocess c.m.s. frame. It is made to ensure that jet-4 and jet-5 will be resolved as separate jets, with full efficiency, by the jet algorithm. Note that some misassignment of energy between jet-4 and jet-5 is tolerable, to the extent that x_3 (and the subprocess c.m.s. energy) are left unaffected.

ii) $|\cos \theta_3| < 0.6$, $30^\circ < |\psi| < 150^\circ$. These cuts guarantee that all three jets are well separated in angle from the incoming parton axis in the subprocess c.m.s. frame.

For three-jet events the total subprocess c.m.s. energy is taken to be the three-jet mass ($\sqrt{\hat{s}} = m_{3J}$), computed using the full corrected 4-vectors of the three highest p_T jets. To ensure good trigger/filter efficiency for the three-jet events and to make a comparison with the corresponding two-jet sample, we require $m_{3J} > 150$ GeV.

The final three-jet sample comprises 173 three-jet events. For events in the sample, the mean separation ($\langle \Delta R_{\min} \rangle$) between the two closest jets in pseudorapidity azimuth space [$\Delta R = \sqrt{(\Delta\eta)^2 + \Delta\phi^2}$], where $\Delta\eta$ is the separation in pseudorapidity and $\Delta\phi$ is the separation in azimuthal angle measured around the beams] is given by $\langle \Delta R_{\min} \rangle \simeq 1.7$ rad. The mean transverse momentum of the highest p_T jet in each event (typically jet-3) is ≈ 55 GeV. The mean transverse momentum of the third highest p_T jet (typically jet-5) is ≈ 25 GeV.

As a cross-check on the performance of the jet algorithm and on the efficacy of the cuts, all events in the three-jet sample were scanned by physicists using the interactive graphics facility. A typical three-jet event is shown in Fig. 3. On the basis of purely subjective criteria, 143 events (83% of the three-jet sample) were classified as having a clear three-jet topology with all three-jets completely resolved from each other and from the beams. In fact the majority of the remaining events were also fully consistent with a three-jet topology but were described as partially resolved, implying that some algorithm dependence might reasonably be expected to enter with respect to the assignment of the detected energy to the parent jets. A total of nine events in the three-jet sample also satisfy the selection criteria for two-jet events, and appear in the two-jet sample at a lower mass ($m_{2J} < m_{3J}$). Note that four-jet events are not actively antiselected: several clear four-jet events were identified in the scan and have been retained in the three-jet sample.

The three-jet Dalitz plot (x_3 versus x_4) for events in the three-jet sample is shown in Fig. 4. The density of events on the Dalitz plot is significantly non-uniform over the range explored. In particular the density of events increases visibly with increasing x_4 , for fixed x_3 ($x_3 \approx 0.85$), as the two-jet region ($x_3 \rightarrow 1, x_4 \rightarrow 1$) is approached. Less apparent, but also significant, is the increase in density of events with x_3 for fixed x_4 ($x_4 \approx 0.6-0.8$). This effect signals the contribution of quasi-collinear final-state bremsstrahlung processes in the data, which are expected to dominate for $x_3 \rightarrow 1$. The projections of the Dalitz plot onto the x_3 and x_4 axes are also shown. The solid curves, which have been normalized to the data, show the predicted distributions in x_3 and x_4 based on the single QCD bremsstrahlung formulae. The dominant subprocesses are predicted to have a very similar x_3, x_4 dependence over this range, and the curves shown have been suitably averaged over the contributing subprocesses. The broken curves show the corresponding phase-space distributions computed assuming a constant matrix element. The data are clearly consistent with the predictions of the single QCD bremsstrahlung formulae, and are inconsistent with the phase-space distributions.

The three-jet angular distribution (ψ versus $\cos \theta_3$) is shown in Fig. 5. The sign of $\cos \theta_3$ has been defined with reference to the direction of the 'fast' and 'slow' incoming partons. Since, in general, the magnitudes of the longitudinal momenta of the incoming partons are not equal in the laboratory frame, the direction of the longitudinal motion of the three-jet system in the laboratory frame uniquely identifies the 'fast' and 'slow' incoming partons. The sign of $\cos \theta_3$ has been defined to be positive when, in the c.m.s. frame, jet-3 points along the direction of the 'fast' incoming parton. Similarly, ψ is defined such that $\psi = 0^\circ$ when jet-4 lies in the plane defined by jet-3 and the incoming parton axis, and points along the direction of the 'fast' incoming parton. Note that the distribution in the angle ψ is symmetric ($\psi \rightarrow -\psi$) and has been folded and plotted from $|\psi| = 0^\circ$ to $|\psi| = 180^\circ$. The advantage of these definitions is that the distributions are then potentially sensitive to forward-backward

asymmetries, which are expected to be present for $2 \rightarrow 3$ processes involving qg (or $\bar{q}g$) initial states as discussed by Combridge and Maxwell¹⁰. For the present choice of cuts the predicted asymmetry $A(\cos \theta_3) [\approx -A(|\psi| - 90^\circ)]$ is very small, $\approx + 1\%$. In Figs. 4 and 5 the projections have been corrected for acceptance losses due to a vertical gap in the calorimetry. The theoretical curves, which have been normalized to the data, show the scaling predictions of the single QCD bremsstrahlung formulae.

The distribution in $\cos \theta_3$ shows a pronounced forward-backward peaking which is similar to the behaviour of the two-jet angular distribution (Fig. 2a) and is in agreement with the predictions of the QCD bremsstrahlung formulae. No significant forward-backward asymmetry is observed [$A(\cos \theta_3) = 0.11 \pm 0.07$]. The data also show a distinct ψ dependence. Configurations for which jet-4 and jet-5 lie close to the plane defined by jet-3 and the beams ($|\psi| \approx 30^\circ, 150^\circ$) are preferred relative to configurations for which $|\psi| \approx 90^\circ$. This effect signals the contribution of initial-state bremsstrahlung processes and is in agreement with the predictions of the QCD bremsstrahlung formulae. Again, no significant forward-backward asymmetry is observed [$A(|\psi| - 90^\circ) = 0.11 \pm 0.07$]. Finally, we note that the agreement between the data and the theoretical curves (Fig. 5) is only qualitative. In particular the measured angular distribution have a tendency to be steeper than the scaling curves. It is perhaps not unreasonable to suppose that, as in the two-jet case, the inclusion of scale-breaking corrections in the theoretical curves would improve the agreement between theory and experiment.

4. THE THREE-JET/TWO-JET RATIO AND THE DETERMINATION OF α_s

In QCD the relative yield of three-jet and two-jet events is directly related to the value of α_s . Integrating the differential cross-sections [Eqs. (1) and (2)] over the dimensionless variables, taking into account the cuts (i) and (ii) above, gives

$$\sigma_{2J} = C_{2J} \alpha_s^2 / \mathfrak{S} \quad (4)$$

$$\sigma_{3J} = C_{3J} \alpha_s^3 / \mathfrak{S} \quad (5)$$

where C_{2J} and C_{3J} are dimensionless coefficients which depend on the subprocess, e.g. $gg \rightarrow gg$, $gg \rightarrow ggg$, etc., and on the choice of cuts. The numerical values of C_{2J} and C_{3J} appropriate to the above (loose) cuts and to an alternative set of (tight) cuts, corresponding to a reduced angular acceptance, are listed in Table 1 for the various possible incoming parton combinations. The values given in Table 1 refer to the dominant elastic and single-gluon production subprocesses only (see footnote to Table 1) but have been calculated using the exact (leading-order) theoretical expressions for the subprocess cross-sections^{3,4}.

As may be seen from Table 1, the two-jet cross-sections follow the well-known rule: $\sigma(gg):\sigma(qg):\sigma(q\bar{q}) \approx 1:(4/9):(4/9)^2$, depending on the incoming parton combination. Remarkably the corresponding three-jet cross-sections are seen to be in essentially the same proportions (to within $\pm 25\%$). This has the important consequence that the three-jet to two-jet ratio is predicted to be almost independent of the incoming parton combination, and ensures that to a first approximation the same effective structure function is relevant for three-jet and two-jet production^{10,11}.

From Eqs. (4) and (5), averaging over the possible incoming parton combinations, the three-jet/two-jet ratio may be written:

$$\sigma_{3J}/\sigma_{2J} = \langle C_{3J}/C_{2J} \rangle \alpha_s. \quad (6)$$

The relative weights of the different incoming parton combinations are given in Section 2 above. As a function of mass the proportion of gg events falls slowly, whilst the proportion of $q\bar{q}$ events rises to compensate. The proportion of qg events is expected to be rather constant over this mass range. Although the exact values of the above relative weights depend somewhat on the parametrization (and on the value of Λ) used to extrapolate the structure function measurements, the value of $\langle C_{3J}/C_{2J} \rangle$ is clearly insensitive to such effects. In the subsequent comparison of theory with experiment, we use the values of the relative weights given above together with the values of C_{3J}/C_{2J} listed in Table 1 to compute $\langle C_{3J}/C_{2J} \rangle$. It has been verified that the error in $\langle C_{3J}/C_{2J} \rangle$ introduced by taking into account only the dominant subprocesses, and due to the uncertainties in the relative weights discussed above, is at the level of a few percent only¹²⁾.

The ratio of three-jet and two-jet cross-sections measured in this experiment is plotted in Fig. 6a as a function of the laboratory rapidity y of the three-jet (or two-jet) system. The same ratio is plotted in Fig. 6b as a function of the subprocess c.m.s. energy ($\sqrt{\hat{s}} = m_{3J}, m_{2J}$). The cross-section ratio has been calculated from the raw event-rate ratio, incorporating a correction ($\approx +20\%$) to account for the difference in ϕ -acceptance for three-jet and two-jet events.

The ratio of three-jet and two-jet cross-sections measured in this experiment is plotted in Fig. 6a as a function of the laboratory rapidity y of the three-jet (or two-jet) system. The same ratio is plotted in Fig. 6b as a function of the subprocess c.m.s. energy ($\sqrt{\hat{s}} = m_{3J}, m_{2J}$). The cross-section ratio has been calculated from the raw event-rate ratio, incorporating a correction ($\approx +20\%$) to account for the difference in ϕ -acceptance for three-jet and two-jet events. In Fig. 6 the errors plotted are entirely statistical. Systematic effects tend to cancel in the calculation of the ratio (e.g. luminosity, trigger/filter efficiencies, etc.). In particular, uncertainties in the calibration of the jet energy scale and in the effects of energy resolution smearing, lead to large uncertainties in the individual event rates, but have a much smaller effect on the event-rate ratio. The estimated systematic error in the three-jet/two-jet ratio, due to possible residual differences in the energy scale and in the resolution for three-jet and two-jet events, is $\pm 15\%$. Systematic errors due to ambiguities in the sample definitions (e.g. treatment of four-jet events) and algorithm-dependent effects (see Section 3) are believed to be somewhat less important, amounting to $\approx \pm 10\%$.

On the basis of the data shown in Fig. 6, we conclude that the three-jet/two-jet ratio shows no significant dependence on rapidity or on subprocess c.m.s. energy over this range.

Further comparison between theory and experiment is somewhat complicated by the theoretical uncertainty related to the freedom of choice of Q^2 -scale appropriate to three-jet and two-jet production. If the relevant Q^2 -scale for two-jet production (Q_{2J}^2) is taken to be $-\hat{t}$, as is consistent with the data on the two-jet angular distribution (see Section 2), then for the two-jet sample defined by the loose cuts above we find $\langle Q_{2J} \rangle \approx 0.45 m_{2J}$ ($Q = \sqrt{\bar{Q}^2}$). Assuming that the Q^2 -scales for the three-jet and two-jet samples are identical, i.e. $\langle Q_{3J} \rangle = 0.45 m_{3J}$, then Eq. (6) may be applied directly to predict the three-jet/two-jet ratio. In Fig. 6 the solid curve shows the expected value of the ratio calculated from Eq. (6) assuming $\alpha_s(Q^2) = 12 \pi / [21 \ln(Q^2/\Lambda^2)]$, i.e. assuming six effective quark flavours and taking $\Lambda = 0.2$ GeV. If the Q^2 -scales for three-jet and two-jet production are not identical, then Eq. (6) will acquire a correction due to the non-cancellation of the common factor α_s^2 in Eqs. (4) and (5) (and due to the non-cancellation of the effective structure function) as a result of the scaling deviations. By way of example, in Fig. 6 the broken curve represents the expected modification of the prediction Eq. (6), assuming $\langle Q_{3J} \rangle = 0.30 m_{3J}$. On the basis of these comparisons, and assuming the validity of the expression for $\alpha_s^2(Q^2)$ given above, we conclude that the three-jet sample is probably characterized by a

lower Q^2 -scale than the corresponding two-jet sample at the same subprocess c.m.s. energy. This result should perhaps not be considered surprising: indeed one might argue *a priori* that, for comparable angular acceptance, the Q^2 -scale is naturally lower in the case where the available energy is shared among a larger number of final-state quanta.

Finally, the data are used to obtain information on the value of α_s . Table 2 summarizes the measured event rates and the corresponding event rate ratios for the loose cuts and for the tight cuts defined in Table 1. The mean value of Q_{2J}/m_{2J} for the two-jet sample is also given on the assumption that $Q_{2J}^2 = -\hat{t}$. In the final column we give the values of α_s computed from Eq. (6), i.e. on the assumption that the Q^2 -scales for the three-jet and two-jet samples are identical. The values of α_s obtained by comparing the three-jet and two-jet samples within the loose and the tight cuts are consistent with each other, but are somewhat higher than might be expected by extrapolating measurements of α_s from lower energies^{13,14}. Since, as we have seen, there may be (and probably are) substantial scale-breaking corrections (quite possibly $\approx -30\%$) to be applied to the values given here, this discrepancy is not pursued further at this time.

In Table 2 a third comparison is made in which the three-jet sample satisfying the tight cuts is compared with a two-jet sample consisting of those two-jet events which satisfy the loose cuts but fail the tight cuts (i.e. two-jet events with $\cos \theta$ in the range 0.6 to 0.8). By deliberately comparing the 'softer' (lower- Q^2) subset of the two-jet sample with what is presumably the 'harder' subset of the three-jet sample, we hope to match the Q^2 -scales of the three-jet and two-jet samples to minimize the magnitude of the scale-breaking correction discussed above. On the basis of this comparison, we obtain a significantly lower value for α_s . From Table 2 we have

$$\alpha_s (K_{3J}/K_{2J}) = 0.16 \pm 0.02 \pm 0.03. \quad (7)$$

The corresponding value of Q^2 ($Q^2 \equiv Q_{2J}^2 \equiv -\hat{t}$) is $\approx 4000 \text{ GeV}^2$. In Eq. (7) the systematic error quoted includes only the experimental systematic uncertainty in the measured three-jet/two-jet ratio discussed above. The unknown residual scale-breaking (and/or higher-order) correction to the theoretical three-jet/two-jet ratio, appropriate to this comparison, is represented by the factor K_{3J}/K_{2J} which has been inserted in the left-hand side of Eq. (7) (and in Table 2). Clearly this factor cannot be eliminated until the next-to-leading-order corrections to the two-jet and three-jet cross-sections have been calculated theoretically.

Acknowledgements

The UA1 Collaboration acknowledges informative discussions with G. Altarelli, L. Pancheri and W.J. Stirling on the material presented above.

I wish to express my personal thanks to all my collaborators on the UA1 experiment especially Professor C. Rubbia for the opportunity to present this data, and to the Workshop Organizing Committee for the invitation to come to Tsukuba.

References

1. Arnison, G. et al. (UA1 Collaboration), Phys. Lett. **136B**, 294 (1984).
2. Bagnaia, P. et al. (UA2 Collaboration), Phys. Lett. **144B**, 283 (1984).
3. Combridge, B. et al., Phys. Lett. **70B**, 234 (1977).
4. Berends, F. et al., Phys. Lett. **103B**, 124 (1981).
Gottschalk, T. and Sivers, D., Phys. Rev. **D21**, 102 (1980).
5. Buckley, E.J. and Kozanecki, W., UA1 Technical Note, TN-85-08 (1985).
6. Combridge, B.L. and C.J. Maxwell, Nucl. Phys. **B239**, 428 (1984).
7. Abramowicz, H. et al., Z. Phys. **C12**, 289 (1982).
Bergsma, F. et al., preprint CERN-EP/84-143.
8. Ellis, R.K. et al., Nucl. Phys. **B173**, 397 (1980).
Antoniou, N.G. et al., Phys. Lett. **128B**, 257 (1983).
9. Angelis, A.L.S. et al., CCOR Collaboration, Nucl. Phys. **B209**, 284 (1982).
10. Combridge, B.L. and Maxwell, C.J., Phys. Lett. **151B**, 299 (1985).
11. Kunszt, Z. and Piétarinen, E., Nucl. Phys. **B164**, 45 (1980).
12. Stirling, W.J. (private communication).
13. Adeva, B. et al., Phys. Rev. Lett. **54**, 1750 (1985).
Althoff, M. et al., Z. Phys. **C26**, 157 (1984).
14. Møller, R. (AFS Collaboration), Niels Bohr Institute preprint NBI-HE-84-34, presented at the 15th Symposium on Multiparticle Dynamics, Lund, 1984.

Table 1

Summary of three-jet and two-jet cross-section coefficients [Eqs. (3) and (4)],
calculated from the formulae of Berends et al.⁴⁾ and Combridge et al.,³⁾

	Loose cuts			Tight cuts		
	3-jet: $x_3 < 0.9$, $ \cos \theta_3 < 0.6$ $30^\circ < \psi < 150^\circ$ 2-jet: $\cos \theta < 0.8$			3-jet: $x_3 < 0.9$, $ \cos \theta_3 < 0.6$ $55^\circ < \psi < 125^\circ$ 2-jet: $\cos \theta < 0.6$		
Parton combination ^{a)}	C_{3J}	C_{2J}	C_{3J}/C_{2J}	C_{3J}	C_{2J}	C_{3J}/C_{2J}
gg	111.5	110.5	1.01	45.3	45.2	1.00
qg	38.1	48.2	0.79	14.8	19.1	0.78
$q\bar{q}$ ^{b)}	16.4	21.4	0.76	6.7	8.4	0.80

a) The cross-sections given refer to the elastic and single-gluon production processes only, e.g. $gg \rightarrow gg$, $gg \rightarrow ggg$, etc.

b) Calculated for identical flavours, e.g. $u\bar{u} \rightarrow u\bar{u}$, $d\bar{d} \rightarrow d\bar{d}$, etc.

Table 2

Summary of three-jet and two-jet event rates and determination of α_s

Samples compared	Number of 3-jets ^{a)}	Number of 2-jets (Q_{2J}/m_{2J})	σ_{3J}/σ_{2J}	$\langle C_{3J}/C_{2J} \rangle$	$\alpha_s(K_{3J}/K_{2J})$
$\frac{\sigma_{3J}(\text{loose})}{\sigma_{2J}(\text{loose})}$	209.2 (173)	1142 0.45	0.183 ± 0.015	0.81	0.226 ± 0.018
$\frac{\sigma_{3J}(\text{tight})}{\sigma_{2J}(\text{tight})}$	66.6 (54)	370 0.56	0.180 ± 0.026	0.81	0.222 ± 0.032
$\frac{\sigma_{3J}(\text{tight})}{\sigma_{2J}(\text{loose}) - \sigma_{2J}(\text{tight})}$	66.6 (54)	772 0.38	0.086 ± 0.012	0.53	0.162 ± 0.024

a) The number of three-jet events has been corrected by $\approx +20\%$ to account for the difference in ϕ -acceptance for three-jet and two-jet events. The raw number of three-jet events is given in parenthesis.

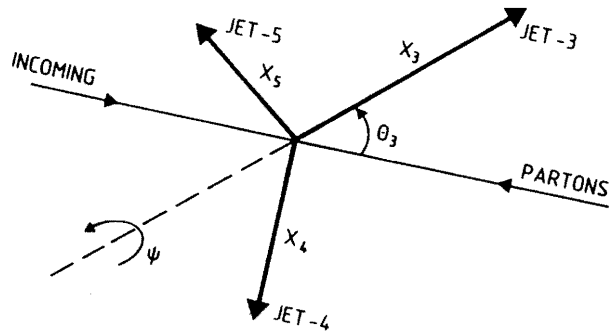


Fig. 1 The three-jet variables defined in the subprocess c.m.s. frame.

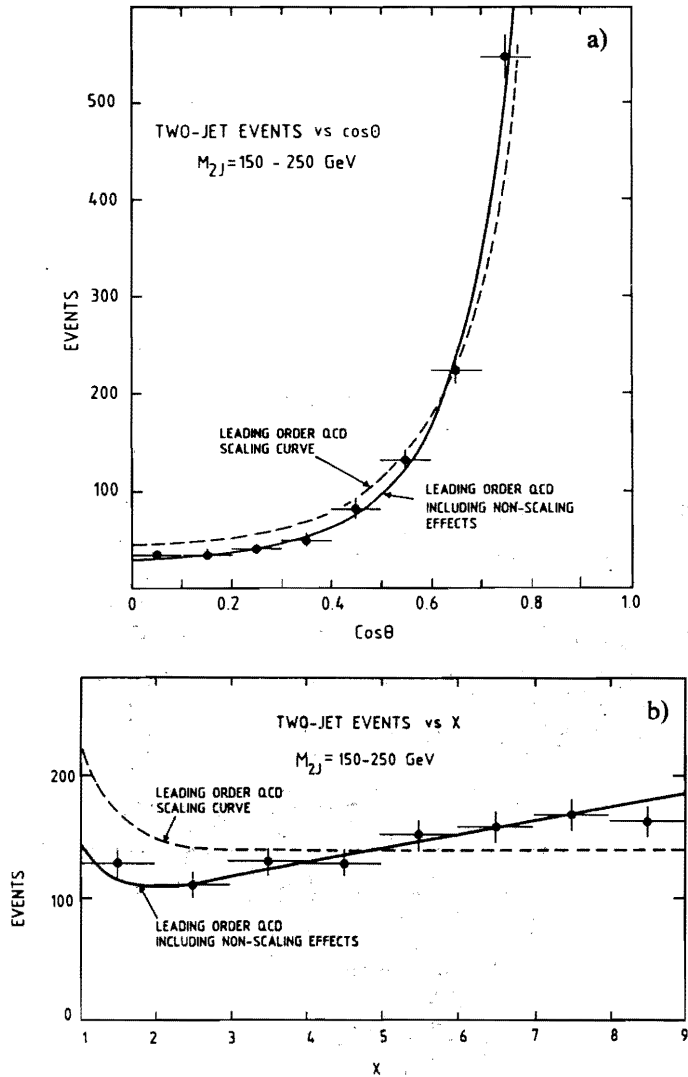


Fig. 2 a) The two-jet angular distribution plotted versus $\cos \theta$. b) The two-jet angular distribution plotted versus $\chi = (1 + \cos \theta)/(1 - \cos \theta)$. The broken curves show the leading-order QCD predictions suitably averaged over the contributing subprocesses, and the solid curves include scale-breaking corrections (see text).

RUN 7020 EVENT 113
THRESHOLDS PT= 1.000 E= 0.100 ET= 1.000

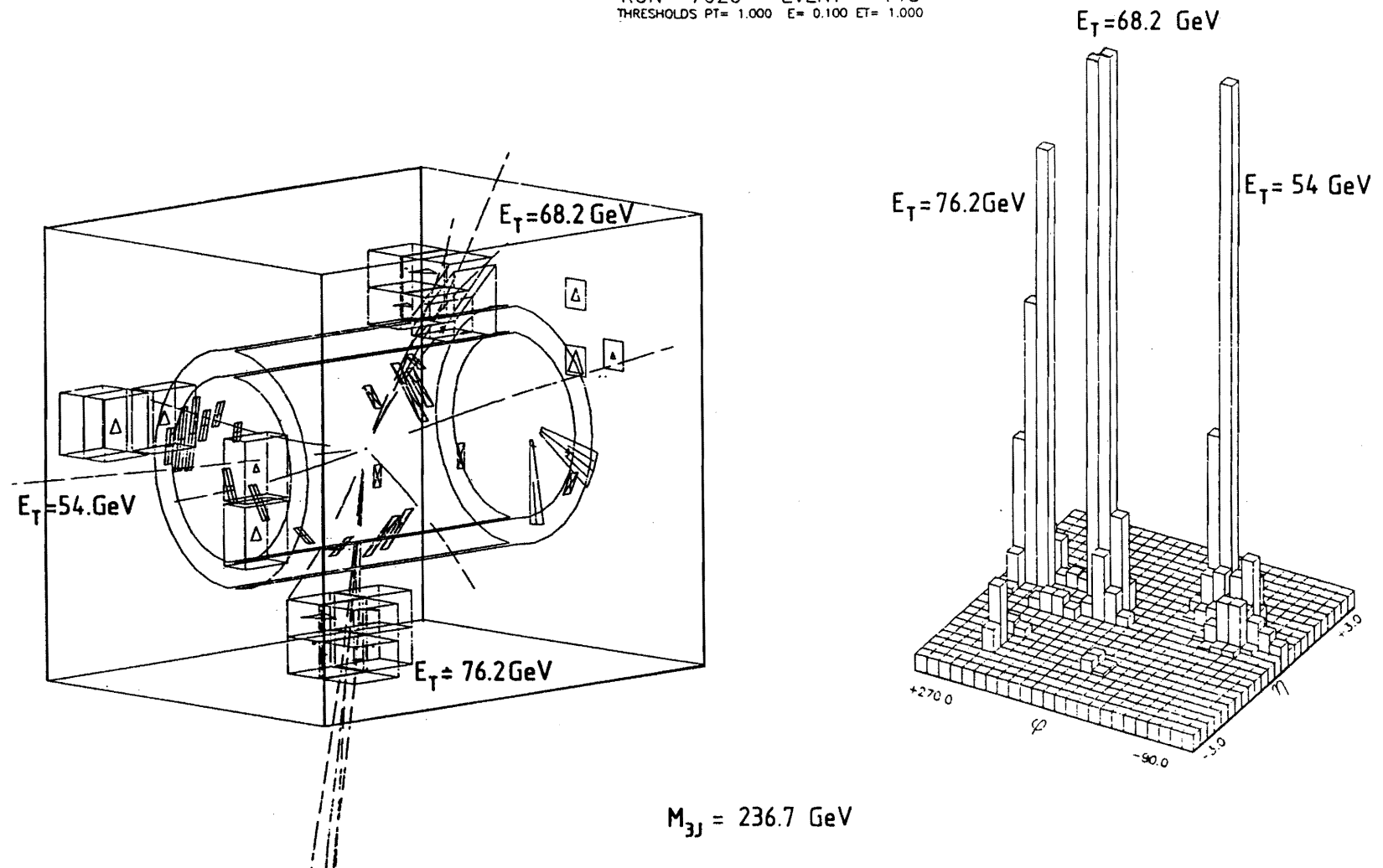


Fig. 3 A typical three-jet event as displayed on the interactive graphics facility.

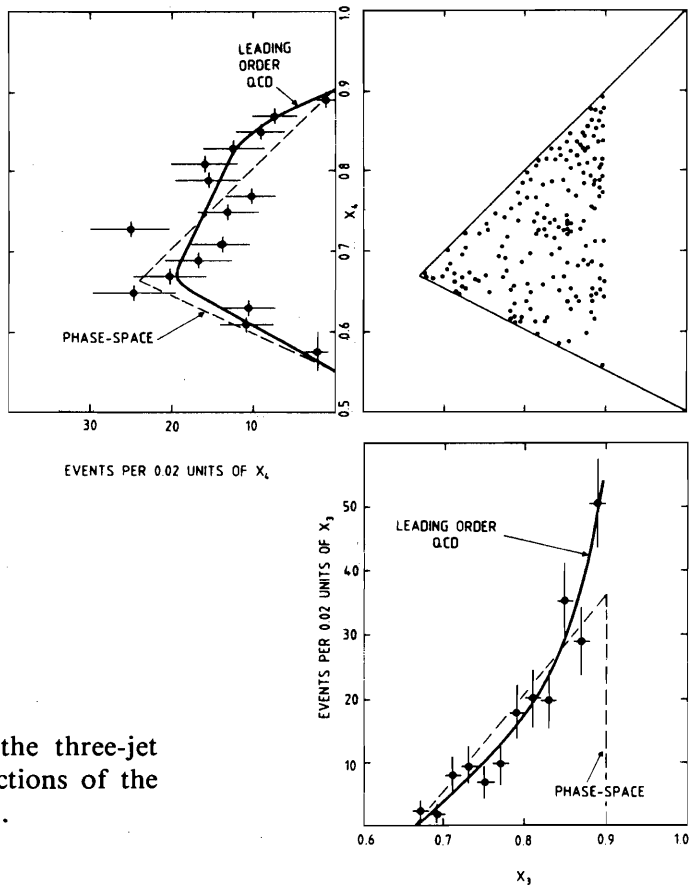


Fig. 4 The Dalitz plot (x_3 versus x_4) for the three-jet sample. The solid curves represent the predictions of the leading-order QCD bremsstrahlung formulae⁴⁾.

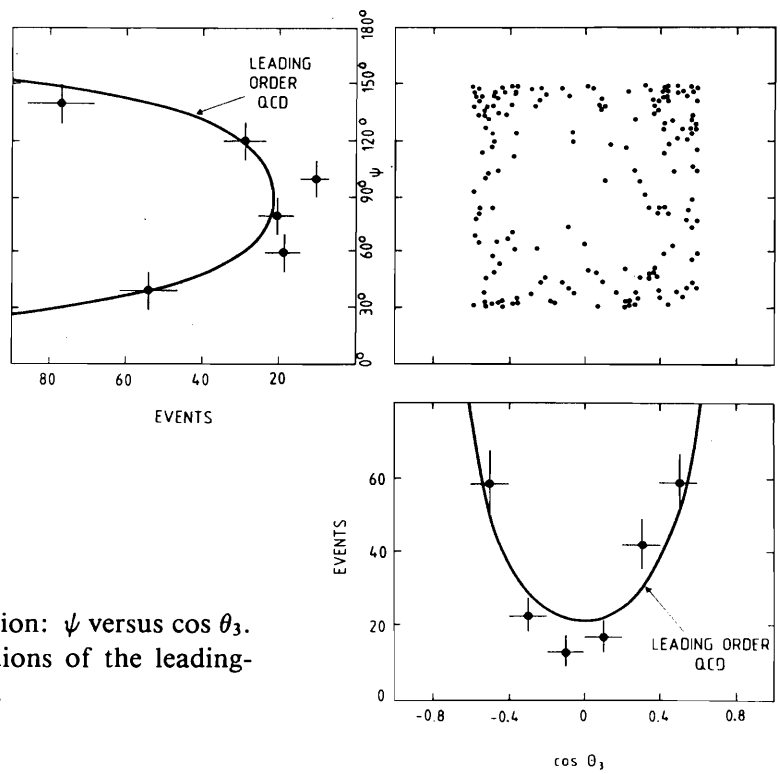


Fig. 5 The three-jet angular distribution: ψ versus $\cos \theta_3$. The theoretical curves are the predictions of the leading-order QCD bremsstrahlung formulae⁴⁾.

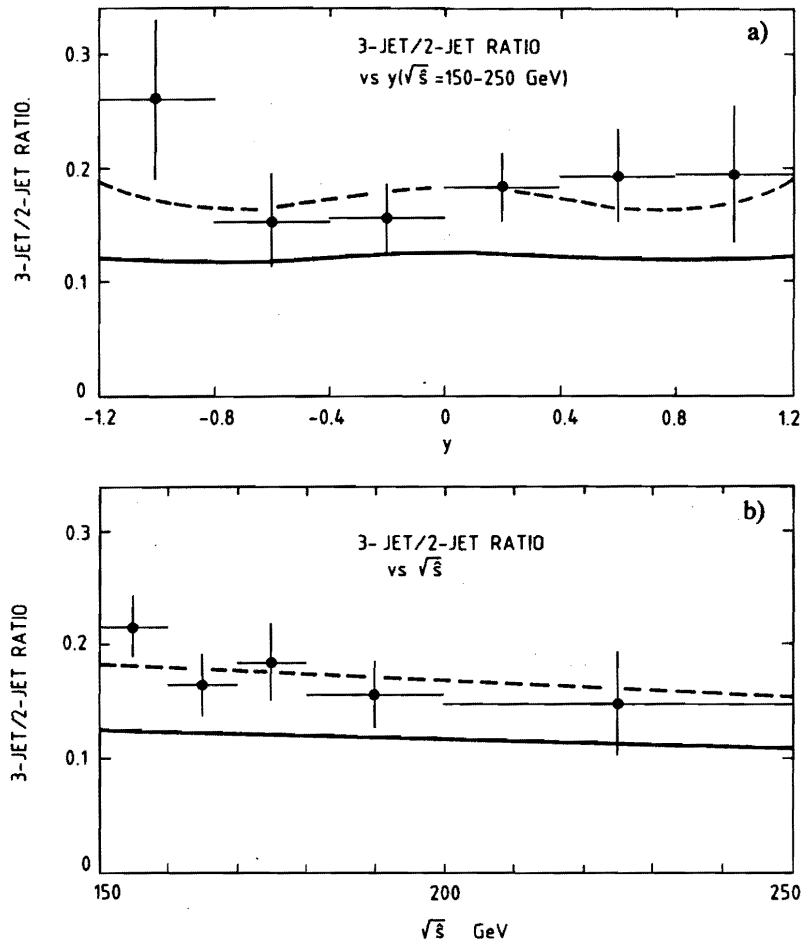


Fig. 6 a) The three-jet/two-jet ratio plotted versus the laboratory rapidity of the three-jet (two-jet) system. b) The three-jet/two-jet ratio plotted versus subprocess c.m.s. energy (mass). The theoretical curves have been calculated assuming six effective quark flavours and taking $\Lambda = 0.2 \text{ GeV}$. The solid curves correspond to the choice of identical Q^2 -scales for the three-jet and two-jet samples: $\langle Q_{2J} \rangle = 0.45 m_{2J}$, $\langle Q_{3J} \rangle = 0.45 m_{3J}$. The broken curves correspond to the choice of a lower Q^2 -scale for the three-jet sample: $\langle Q_{3J} \rangle = 0.30 m_{3J}$.